Chapter 6

Active vibration isolation

6.1 Introduction

There are two broad classes of problems in which vibration isolation is necessary:

1. Operating equipments generate oscillatory forces which can propagate in the supporting structure (Fig.6.1.a).This situation corresponds to that of an engine in a car, or an attitude control reaction wheel assembly in a spacecraft.

2. Sensitive equipments may be supported by a structure which vibrates appreciably (Fig.6.l.b). This situation corresponds to, for example, a telescope in a spacecraft, a precision machine tool in a workshop, or a passenger seated in a car.

The disturbance may be either deterministic, such as the unbalance of a motor, or random as in a passenger car riding on a rough road. As already mentioned, this book is focused on the *feedback* strategies for active isolation; they apply to both deterministic and random disturbances. For deterministic sources such as a rotating unbalance, *feedforward* control can also be very effective (see Fuller et al., chap. 7).

In this chapter, we first consider the single-axis isolation problem; the acceleration feedback (also called "sky-hook" damper) and the force feedback are compared. Next, we consider the general purpose 6-axis isolator based on a Stewart platform. The decentralized integral force feedback of a Stewart platform is examined. The joint pointing/isolation control is also briefly examined. Finally, we consider the application of the sky-hook damper to an active vehicle suspension.

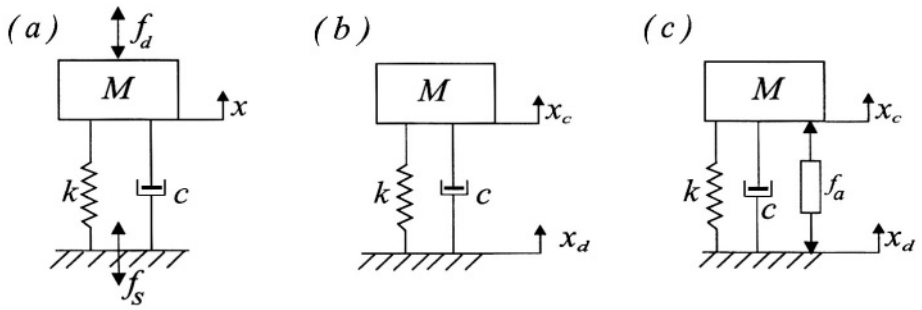

Figure 6.1: *(a) Operating equipment generating a disturbance force f_d. (b) Sensitive equipment supported by a vibrating structure. (c) Conceptual design of an active isolation device.*

6.2 Passive isolator

First, let us consider the situation of an operating equipment generating a disturbance force f_d (Fig.6.1.a). If the support is fixed, the governing equations are as follows:

$$M\ddot{x} + c\dot{x} + kx = f_d \tag{6.1}$$

$$f_s = kx + c\dot{x} \tag{6.2}$$

In the Laplace domain,

$$X(s) = \frac{F_d(s)}{M(s^2 + 2\xi\omega_n s + \omega_n^2)} \tag{6.3}$$

$$F_s(s) = M(\omega_n^2 + 2\xi\omega_n s)X(s) \tag{6.4}$$

where $X(s), F_d(s)$ and $F_s(s)$ stand for the Laplace transform of respectively $x(t), f_d(t)$ and $f_s(t)$, and with the usual notations $\omega_n^2 = k/M$ and $2\xi\omega_n = c/M$. The *transmissibility* of the support is defined in this case as the transfer function between the disturbance force f_d applied to the mass and the force f_s transmitted to the support structure; combining Equ.(6.3) and (6.4), we get

$$\frac{F_s(s)}{F_d(s)} = \frac{1 + 2\xi s/\omega_n}{1 + 2\xi s/\omega_n + s^2/\omega_n^2} \tag{6.5}$$

Next, consider the second situation illustrated in Fig.6.1.b; the disturbance is the displacement x_d of the supporting structure (that we call "dirty body") and the system output is the displacement x_c of the sensitive equipment (referred to as "clean body"). Following a procedure similar to that leading to Equ.(6.5),

it is easily established (Problem P.6.1) that the transmissibility of this isolation system, defined in this case as the transfer function between the displacement of the dirty body and that of the clean body, is given by

$$\frac{X_c(s)}{X_d(s)} = \frac{1 + 2\xi s/\omega_n}{1 + 2\xi s/\omega_n + s^2/\omega_n^2} \tag{6.6}$$

which is identical to Equ.(6.5); the two isolation problems can therefore be treated in parallel. The amplitude of the corresponding *FRF* (for $s = j\omega$) is represented in Fig.6.2 for various values of the damping ratio ξ.

We observe that

- All the curves are larger than 1 for $\omega < \sqrt{2}\,\omega_n$ and become smaller than 1 for $\omega > \sqrt{2}\,\omega_n$. Thus the critical frequency $\sqrt{2}\,\omega_n$ separates the domains of amplification and attenuation of the isolator.

- When $\xi = 0$, the high frequency decay rate is $1/s^2$, that is -40 dB/decade, while very large amplitudes occur near the corner frequency ω_n (the natural frequency of the spring-mass system).

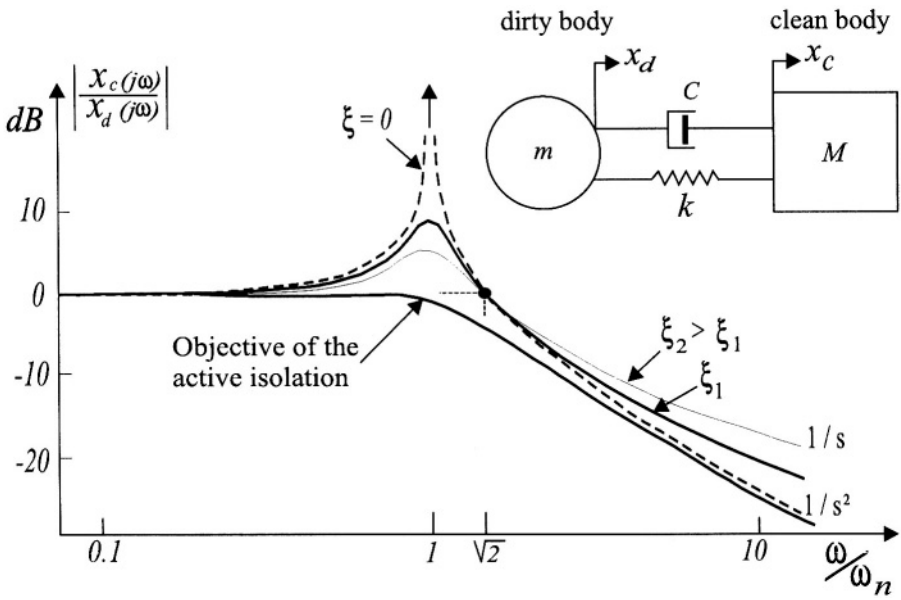

Figure 6.2: *Passive isolator transmissibility FRF for various values of the damping* ξ.

- The damping reduces the amplitude at resonance, but also tends to reduce the effectiveness at high frequency; the high frequency decay rate becomes $1/s$ (-20 dB/decade).

The design of a passive isolator involves a trade-off between the resonance amplification and the high frequency attenuation; the ideal isolator should have a frequency dependent damping, with high damping below the critical frequency $\sqrt{2}\ \omega_n$ to reduce the amplification peak, and low damping above $\sqrt{2}\ \omega_n$ to improve the decay rate. The objective in designing an active isolation system will be to add a force actuator working in parallel with the spring and dash-pot (Fig.6.1.c), that will operate in such a way that there is no amplification below ω_n and the decay rate is -40dB/decade at high frequency, as represented in dotted line in Fig.6.2.

6.3 The "sky-hook" damper

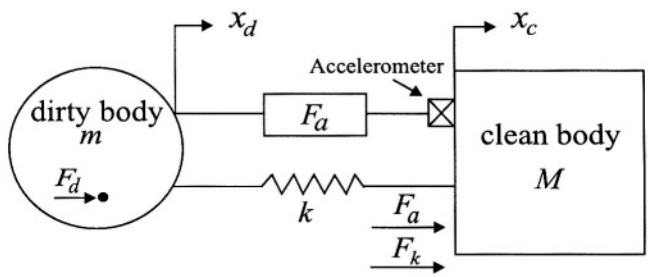

Figure 6.3: *Single axis soft isolator.*

Consider the single axis isolator of Fig.6.3. It consists of a soft spring k acting in parallel with a force actuator generating a control force F_a; the objective is to isolate the clean body from the disturbance F_d applied to the dirty body. With the usual Laplace notations, the equations governing the system are as follows:

- *Dirty body:*

$$X_d(s) = \frac{1}{ms^2}(-F_a - F_k) + \frac{1}{ms^2}F_d \tag{6.7}$$

- *Clean body:*

$$X_c(s) = \frac{1}{Ms^2}(F_a + F_k) \tag{6.8}$$

- *Spring:*

$$F_k = -(X_c - X_d)k \tag{6.9}$$

In the sky-hook isolator, a feedback link is established between the absolute acceleration of the clean body, $s^2 X_c$, and the actuator force F_a, with an integral controller g/s (Fig.6.4.a), leading to a

$$F_a = -\frac{g}{s} s^2 X_c = -gsX_c \tag{6.10}$$

We see that the active control force is proportional to the clean body *absolute* velocity; this is why this control is called "sky-hook" damper (Fig.6.4.b).

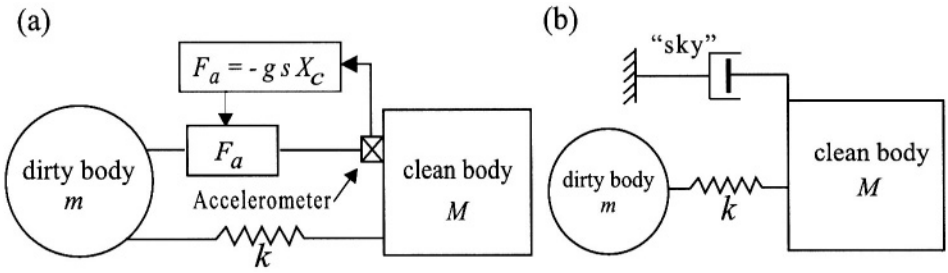

Figure 6.4: *(a) Soft isolator with acceleration feedback. (b) Equivalent "sky-hook" damper.*

Introducing Equ.(6.10) into (6.8) and using Equ.(6.9), we get

$$(Ms^2 + gs + k)X_c = kX_d \tag{6.11}$$

or

$$\frac{X_c(s)}{X_d(s)} = \left[\frac{M}{k}s^2 + \frac{g}{k}s + 1\right]^{-1} \tag{6.12}$$

Thus, the transmissibility has a corner frequency at $\omega_n = \sqrt{k/M}$, its high frequency decay rate is $1/s^2$, that is -40 dB/decade, and the control gain g can be chosen in such a way that the isolator is critically damped ($\xi = 1$); the corresponding value of the gain is $g = 2\sqrt{kM}$. In this way, we achieve a low-pass filter without overshoot with a roll-off of -40 dB/decade. This transmissibility follows exactly the objective represented in Fig.6.2.

Combining Equ.(6.7) to (6.9), the open-loop transfer function of the soft isolator of Fig.6.3 can be written

$$G(s) = \frac{s^2 X_c(s)}{F_a(s)} = \frac{ms^2}{Mms^2 + k(M+m)} \tag{6.13}$$

The open-loop poles are the natural frequencies of the system without control. The rigid body modes do not appear in the transfer function (6.13) because they are not controllable from F_a. The root locus of the closed-loop poles as the gain g of the controller increases is shown in Fig.6.5.

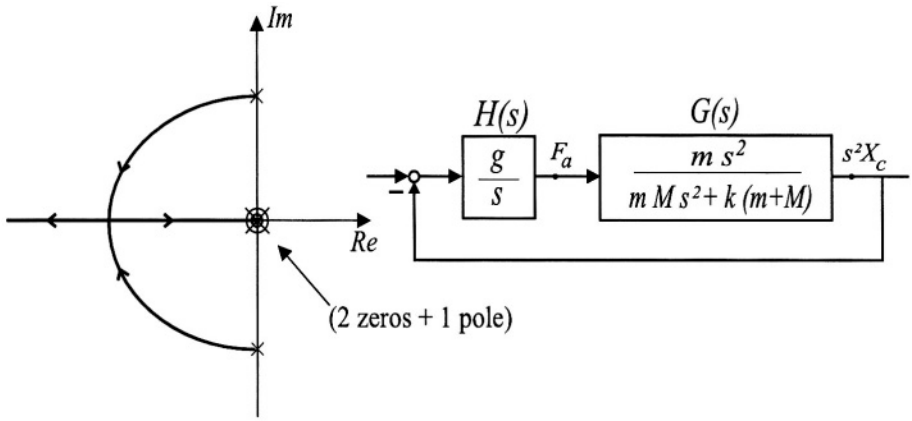

Figure 6.5: *Root locus of the sky-hook damper.*

In developing the sky-hook damper, we have assumed that the passive part involves only a spring. If we include also a dash-pot of constant c, Equ.(6.9) must be replaced by

$$F_k = -(X_c - X_d)(k + cs) \tag{6.14}$$

and Equ.(6.11) becomes

$$[Ms^2 + (g + c)s + k]X_c = (k + cs)X_d \tag{6.15}$$

which shows that the high frequency roll-off is reduced to -20dB/decade. Thus, better performances will be achieved without passive damping (Problem P.6.2).

6.4 Force feedback

If we look at Equ.(6.8), we see that the acceleration of the clean body is proportional to the total force transmitted by the interface, $F = F_a + F_k$. As a result, the sky-hook damper can be obtained alternatively with the control configuration of Fig.6.6, where a force sensor has been substituted to the acceleration sensor. Equations (6.7) to (6.9) still hold and we must add the sensor equation

$$F = F_a + F_k \tag{6.16}$$

It follows that the open-loop transfer function between the actuator force input F_a and the force sensor output F is

$$G(s) = \frac{F}{F_a} = \frac{mMs^2}{mMs^2 + (m+M)k} \tag{6.17}$$

It is identical to Equ.(6.13), except for the constant M relating the total force F to the clean body acceleration. As a result, the root locus of Fig.6.5 also applies to the integral force feedback damper which is totally equivalent to the sky-hook damper. Taking into account the constant M relating the clean body acceleration and the total transmitted force, the transmissibility of the active isolator now reads

$$\frac{X_c}{X_d} = \left[\frac{M}{k}s^2 + \frac{M}{k}gs + 1\right]^{-1} \tag{6.18}$$

which is totally equivalent to Equ.(6.12)(except for the slightly different meaning of g).

The control strategies based on acceleration feedback and on force feedback appear as totally equivalent for the isolation of rigid bodies. However, the force feedback has two advantages which may be significant in some circumstances. The first one is related to sensitivity: force sensors with a sensitivity of $10^{-3}N$ are commonplace and commercially available; if we consider a clean body with a mass of 1000 kg (e.g. a telescope), the corresponding acceleration is $10^{-6}m/s^2$. Accelerometers with such a sensitivity are more difficult to find; for example, the most sensitive accelerometer available in the Bruel & Kjaer catalogue is $2.10^{-5}m/s^2$(model 8318). The second advantage is stability when the clean body is flexible; this is discussed below.

6.5 Flexible clean body

When the clean body is flexible, the behaviour of the acceleration feedback and the force feedback are no longer the same, due to different poles/zeros config-

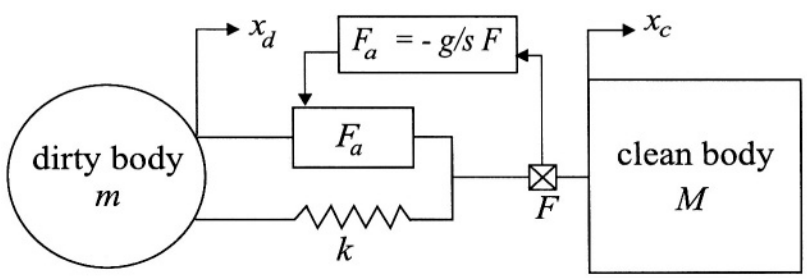

Figure 6.6: *Force feedback isolator.*

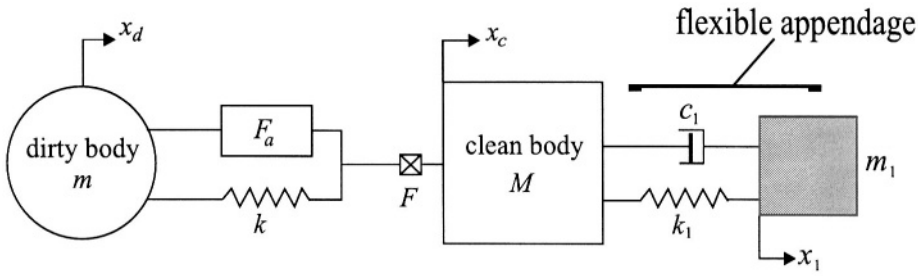

Figure 6.7: *Clean body with a flexible appendage.*

urations of the two control strategies. In fact, different sensor configurations correspond to different locations of the zeros in the s-plane. To analyse this situation, consider the clean body with a flexible appendage as represented in Fig.6.7; the nominal numerical values used in the calculations are $m = 1.1kg$, $M = 1.7kg$, $k = k_1 = 12000N/m$, $c_1 = 0$; the mass m_1 of the flexible appendage is taken as a parameter to analyse the interaction between the flexible appendage and the isolation system. When m_1 is small, the flexible appendage is much more rigid than the isolation system and the situation is not much different from that of a rigid body. Figure 6.8 shows the root locus plots for $m_1 = 0.5kg$; the acceleration feedback and the force feedback have similar root locus plots, with a new pole/zero pair appearing higher on the imaginary axis; the only difference between the two plots is the distance between the pole and the zero which is larger for the acceleration feedback; as a result, the acceleration feedback produces a larger damping of the higher mode. In contrast,

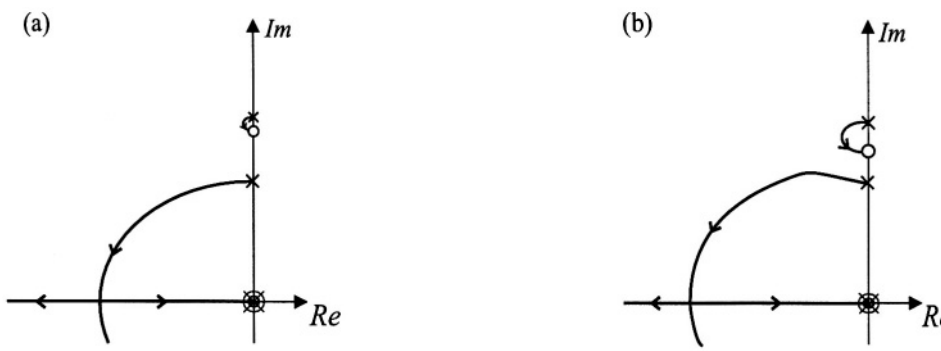

Figure 6.8: *Root locus of the isolation system with a light flexible appendage ($m_1 = 0.5kg$). (a)Force feedback. (b)Acceleration feedback.*

when m_1 is large, the root locus plots are reorganized as shown in Fig.6.9 for $m_1 = 3.5kg$. For force feedback (Fig.6.9.a), the poles and zeros still alternate on

the imaginary axis, leading to a stable root locus; this property is lost for the acceleration feedback (Fig.6.9.b), leading to an unstable loop for the lower mode. In practice, however, this loop is moved slightly to the left by the structural damping, and the control system can still operate for small gains (conditionally stable).

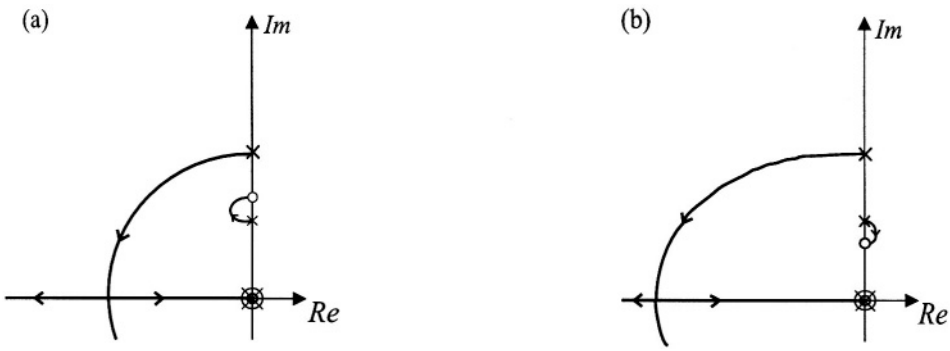

Figure 6.9: *Root locus of the isolation system with a heavy flexible appendage ($m_1 = 3.5kg$). (a)Force feedback. (b)Acceleration feedback.*

6.5.1 Free-free beam with isolator

To analyse a little further the situation when the clean body is flexible, consider the vertical isolation of a free-free continuous beam from the disturbance of a dirty body of mass m (Fig.6.l0.a). This situation is representative of a large space structure with its attitude control system. Note that the rigid body modes are uncontrollable from the internal force F_a. In the numerical example described below, the length of the beam is $l = 5m$, the mass per unit length is $\rho = 2\ kg/m$, the stiffness of the isolator is $k = 1N/m$ and the mass of the dirty body is $m = 1kg$; the stiffness EI of the beam is taken as a parameter.

Let Ω_i be the natural frequencies of the flexible modes of the free-free beam alone (Fig.6.10.b) and Z_i be the transmission zeros corresponding to a force excitation and a collocated displacement sensor (or equivalently acceleration). According to section 2.4, Z_i are the natural frequencies of the system with an additional restraint at the connecting degree of freedom of the isolator. Because of the collocation (Fig.2.5), the poles and zeros are alternating on the imaginary axis, so that Ω_i and Z_i satisfy

$$Z_i < \Omega_i < Z_{i+1} \tag{6.19}$$

Next, consider the complete system (beam + dirty body) and let ω_i be its natural frequencies (flexible mode only, because the rigid body modes are not controllable from the internal force F_a). If the control system uses a force sensor

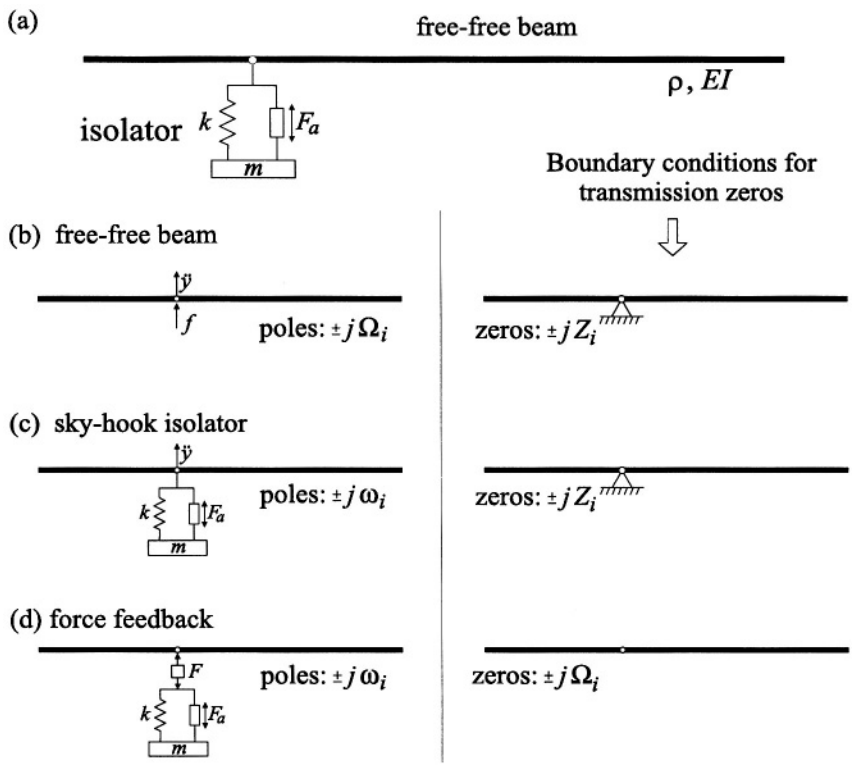

Figure 6.10: *(a) Free-free beam and single axis isolator. The other figures illustrate the various situations and the boundary conditions corresponding to the transmission zeros. (b) Free-free beam with displacement sensor and point force actuator. (c) Free-free beam and sky-hook isolator. (d) Free-free beam and isolator with force feedback.*

(Fig.6.10.d), the transmission zeros, obtained by enforcing a zero force at the connecting d.o.f., are identical to the natural frequencies of the system when the isolator is disconnected from the beam; which are identical to the natural frequencies Ω_i of the free-free beam. It can be shown that the residues in the modal expansion of the *FRF* between the force actuator F_a and the force sensor F are all positive (Problem P.6.4). It follows that the poles and zeros alternate and the following relation holds:

$$\omega_i < \Omega_i < \omega_{i+1} \tag{6.20}$$

This condition guarantees a fixed, interlacing, pole/zero pattern of the open-

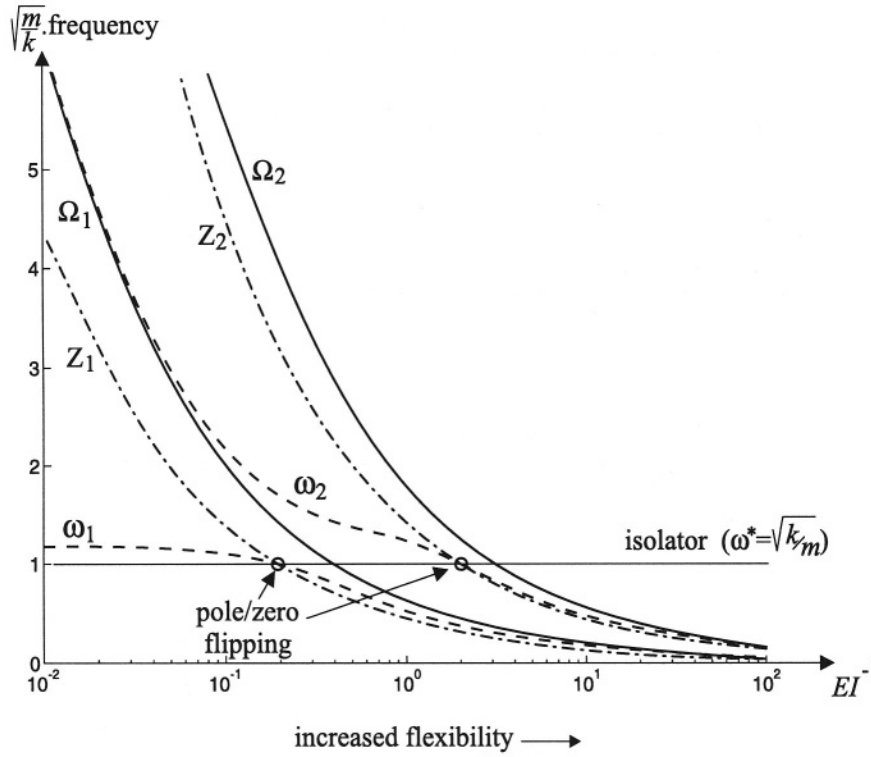

Figure 6.11: *Flexible beam with an isolator; evolution of ω_i,Z_i and ω_i with the flexibility of the beam.*

loop system and the stability of the closed-loop system when a force feedback is used.

With an acceleration feedback (sky-hook damper, Fig.6.10.c) the poles are still $\pm j\omega_i$ while the zeros, obtained by enforcing a zero acceleration at the connecting d.o.f. are $\pm jZ_i$, as for the free-free beam of Fig.6.10.b. This actuator/sensor configuration is no longer collocated, so that no condition similar to (6.19) or (6.20) holds between ω_i and Z_i. When the beam is stiff, the interlacing property $\omega_i < Z_i < \omega_{i+1}$ is satisfied and the stability is guaranteed, but as the beam becomes more flexible, the values of ω_i and Z_i decrease at different rates and a pole/zero flipping occurs when they both become equal to the natural frequency of the isolator $(\omega^* = \sqrt{k/m})$(Fig.6.11). As a result, the system is no longer unconditionally stable when the flexibility is such that $\omega_1 = Z_1 = \omega^* = \sqrt{k/m}$, and above.

As a conclusion to this section, it seems that the sky-hook damper imple-

mentation (acceleration feedback) is preferable when the clean-body is fairly stiff as compared to the isolator corner frequency (e.g. car suspension), to benefit from the better active damping properties of the flexible modes (Fig.6.8). On the contrary, the force feedback implementation looks preferable when the clean body is very flexible (e.g. space structure), to benefit from the guaranteed stability.

6.6 6 d.o.f. isolator

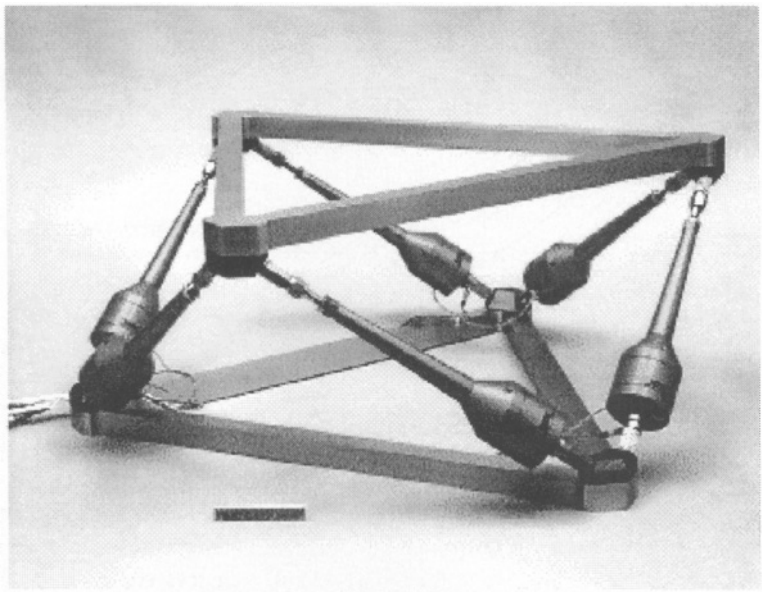

Figure 6.12: *Multi-purpose soft isolator based on a Stewart platform (JPL).*

In the foregoing sections, we have analysed a single axis active isolator which combines a -40 dB/decade attenuation rate in the roll-off region with no overshoot at the corner frequency. To fully isolate two rigid bodies with respect to each other (e.g. an engine from the body of a car, or a telescope from the carrier spacecraft) we would need six such isolators judiciously placed, that could be controlled either in a centralized or (more likely) in a decentralized manner. For a number of space applications, generic multi-purpose 6 d.o.f. isolators have been developed with a standard *Stewart platform* architecture (Fig.6.12).

These general purpose isolators can be used to isolate noisy components such as a reaction wheel assembly (*RWA*) from the rest of the spacecraft (the wheels apply low frequency torques to control the attitude of the spacecraft, but in doing so they also generate undesirable high frequency forces and torques shaking

the base of the structure; this situation is depicted in Fig.6.1.a). Alternatively, they can also be used to isolate quiet subsystems such as a telescope or other sensitive payloads from the carrier spacecraft (Fig.6.1.b). The isolation objectives are illustrated in Fig.6.13; the ideal 6 d.o.f. isolation platform should transmit the attitude control torque within the bandwidth ω_c of the attitude control system and filter all the high frequency disturbances above ω_c.

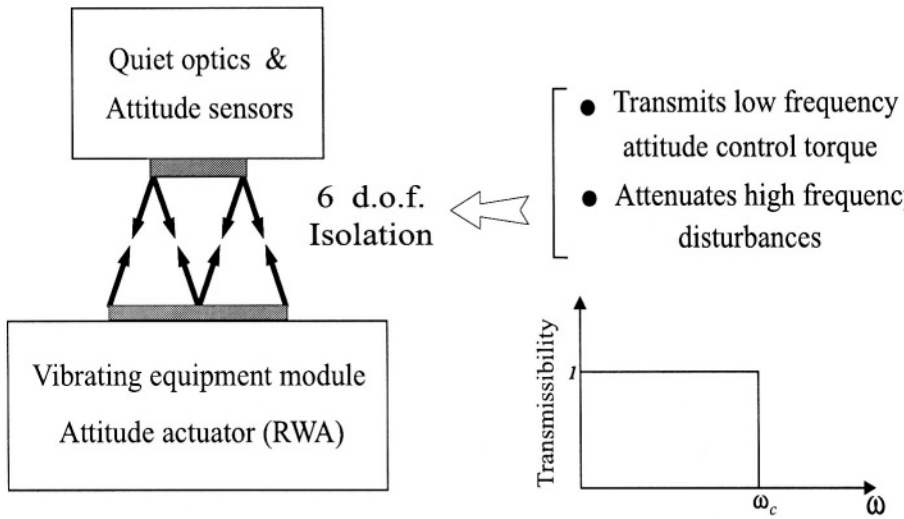

Figure 6.13: *Principle of the 6 d.o.f. vibration isolation and isolation objectives.*

The Stewart platform of Fig.6.12 uses 6 identical active struts arranged in a mutually orthogonal configuration connecting the corners of a cube as indicated in Fig.6.14. The triangular base plate connects the nodes 1,3,5 and the payload plate connect the nodes 2,4,6. This *cubic* architecture is interesting because it provides a uniform control capability in all directions, a uniform stiffness in all directions, and it minimizes the cross-coupling amongst actuators (being orthogonal to each other). It also tends to minimize the spread of modal frequencies.

Figure 6.14 depicts the geometry of the hexapod and the numbering system for the nodes and the struts; the basic frame $\{x_b, y_b, z_b\}$ has its origin at node 0; the reference (or payload) frame $\{x_r, y_r, z_r\}$ has its origin at the geometrical center of the hexapod, noted as node 8, and $\vec{z}_r$ is perpendicular to the payload plate; the orientation of $\vec{x}_r$ and $\vec{y}_r$ is shown in Fig.6.14. If we neglect the flexibility of the struts and the bending stiffness of the flexible joints connecting the struts to the base and payload plates, the dynamic equations of motion can be obtained from rigid body dynamics.

If the base is fixed and the payload is an axisymmetrical rigid body of mass m with the principal axes of inertia aligned with $\{x_r, y_r, z_r\}$, principal moment

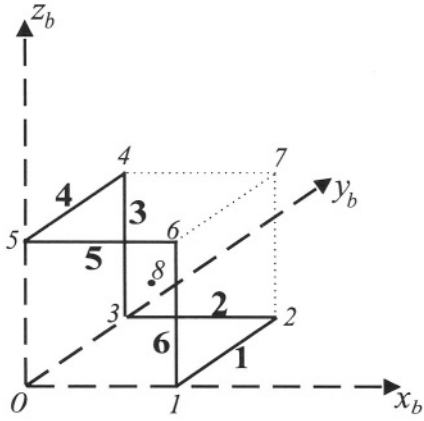

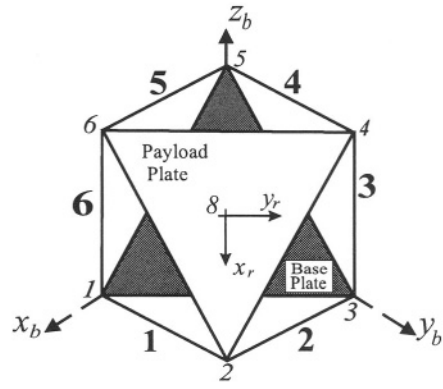

node 0 : (0,0,0) node 4 : (0,L,L)
node 1 : (L,0,0) node 5 : (0,0,L)
node 2 : (L,L,0) node 6 : (L,0,L)
node 3 : (0,L,0) node 7 : (L,L,L)
node 8 : (L/2, L/2, L/2)

z_r station of payload plate = $L/2\sqrt{3}$

z_r station of base plate = $-L/2\sqrt{3}$

Figure 6.14: *Geometry and coordinate systems for the cubic hexapod isolator. Numbers in bold indicate the active struts.*

of inertia $I_x = I_y = mR_x^2$, $I_z = mR_z^2$, and with the center of mass located at an offset distance Z_c from the geometrical center, along the vertical axis z_r, the dynamic equation (for small rotations) of the isolator is

$$M\ddot{x} + Kx = Bu \tag{6.21}$$

where $x = (x_r, y_r, z_r, \theta_x, \theta_y, \theta_z)^T$ is the vector describing the small displacements and rotations in the payload frame $\{x_r, y_r, z_r\}$, $u = (u_1, ...u_6)^T$ is the vector of active control forces in strut 1 to 6 respectively, M and K are the mass and stiffness matrices of the isolator, given by

$$M = m \begin{pmatrix} 1 & 0 & 0 & 0 & Z_c & 0 \\ 0 & 1 & 0 & -Z_c & 0 & 0 \\ 0 & 0 & 1 & 0 & 0 & 0 \\ 0 & -Z_c & 0 & (R_x^2 + Z_c^2) & 0 & 0 \\ Z_c & 0 & 0 & 0 & (R_x^2 + Z_c^2) & 0 \\ 0 & 0 & 0 & 0 & 0 & R_z^2 \end{pmatrix} \tag{6.22}$$

$$K = kBB^T = k\ diag(2, 2, 2, 0.5L^2, 0.5L^2, 2L^2) \tag{6.23}$$

where k is the stiffness of one strut. B is the influence matrix of the active control force:

$$B = \frac{1}{\sqrt{6}} \begin{pmatrix} 1 & 1 & -2 & 1 & 1 & -2 \\ \sqrt{3} & -\sqrt{3} & 0 & \sqrt{3} & -\sqrt{3} & 0 \\ \sqrt{2} & \sqrt{2} & \sqrt{2} & \sqrt{2} & \sqrt{2} & \sqrt{2} \\ -L/2 & L/2 & L & L/2 & -L/2 & -L \\ -L\sqrt{3}/2 & -L\sqrt{3}/2 & 0 & L\sqrt{3}/2 & L\sqrt{3}/2 & 0 \\ L\sqrt{2} & -L\sqrt{2} & L\sqrt{2} & -L\sqrt{2} & L\sqrt{2} & -L\sqrt{2} \end{pmatrix} \tag{6.24}$$

(B is the transposed of the Jacobian J between the small displacements and rotations δx and the length increments δq of the legs; $\delta q = J\delta x$; L is the length of the struts). The proof of Equ. (6.21) to (6.24) is left as an exercise (Problem P.6.5).

The natural frequencies of the isolator and its payload can be obtained by solving the eigenvalue problem on the left side of Equ. (6.21); the z-translation or "bounce" mode and the z-rotation or "torsional" mode are decoupled, with natural frequencies given by

$$\Omega_3 = \sqrt{2}\,\Omega_0 \qquad\qquad \Omega_6 = \frac{\sqrt{2}}{\rho_z}\Omega_0 \tag{6.25}$$

where $\Omega_0 = \sqrt{k/m}$ and $\rho_z = R_z/L$ is the z-axis radius of gyration normalized to the strut length. For most cases, $\rho_z < 1$ and $\Omega_6 > \Omega_3$. The remaining four modes are lateral bending coupled with shear; their natural frequencies occur in two identical pairs, solutions of the characteristic equation

$$\left(2 - \frac{\Omega^2}{\Omega_0^2}\right)\left(\frac{1}{2} - \rho_x^2\frac{\Omega^2}{\Omega_0^2}\right) - 2\rho_c^2\frac{\Omega^2}{\Omega_0^2} = 0 \tag{6.26}$$

where $\rho_x = R_x/L$ is the x-axis radius of gyration normalized to the strut length and $\rho_c = Z_c/L$ is the center of mass offset normalized to the strut length. Note that if the center of mass is at the geometric center ($\rho_c = 0$) and if $\rho_x = \frac{1}{2}$ and $\rho_z = 1$, the hexapod will have 6 identical natural frequencies, all equal to Ω_3.

6.7 Decentralized control of the 6 d.o.f. isolator

Let us assume that each leg is equipped with a force sensor as in Fig.6.6; since each leg consists of a passive spring of stiffness k in parallel with a force actuator, the output equation reads

$$y = -kq + u \tag{6.27}$$

where $y = (y_1, \ldots y_6)^T$ is the vector containing the 6 force sensor outputs, q is the vector of leg extensions from the equilibrium position, k is the strut stiffness and $u = (u_1, \ldots u_6)^T$ is the vector of active control forces. Taking into account

the relationship between the leg extension and the payload frame displacement, $q = Jx = B^T x$, we have

$$y = -kB^T x + u \tag{6.28}$$

Once again, we note that the same matrix B appears in Equ.(6.21) and (6.28) because the sensors and actuators are collocated. Using a decentralized integral force feedback with constant gain g, we find the controller equation

$$u = -\frac{g}{s} y \tag{6.29}$$

Combining Equ.(6.21), (6.28) and (6.29), we obtain the closed-loop equation

$$Ms^2 x + Kx = \frac{g}{s+g} kBB^T x$$

and, taking into account that $K = kBB^T$,

$$[Ms^2 + K\frac{s}{s+g}]x = 0 \tag{6.30}$$

If we transform into modal coordinates, $x = \Phi z$, and take into account the orthogonality relationships (2.8) and (2.9), the characteristic equation is reduced to a set of uncoupled equations

$$\left(s^2 + \Omega_i^2 \frac{s}{s+g}\right) z_i = 0 \tag{6.31}$$

Thus, every mode follows the characteristic equation

$$s^2 + \Omega_i^2 \frac{s}{s+g} = 0$$

or

$$1 + g\frac{s}{s^2 + \Omega_i^2} = 0 \tag{6.32}$$

The corresponding root locus is shown in Fig.6.15. It is identical to Fig.6.5 for a single-axis isolator; however, unless the 6 natural frequencies are identical, a given value of the gain g will lead to different pole locations for the various modes and it will not be possible to achieve the same damping for all modes. This is why it is recommended to locate the payload in such a way that the spread of the modal frequencies is minimized.

6.7.1 Remarks

(i) The foregoing model is based on the assumption that there is no structural damping and that the only contribution to the stiffness matrix is the axial

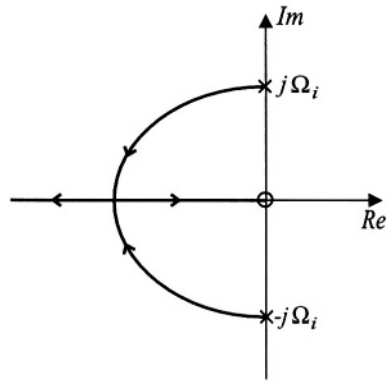

Figure 6.15: *Root locus of the modes of the six-axis isolator with integral force feedback.*

stiffness of the struts, so that $K = kBB^T$. In practice, however, the spherical joints at the connection between the legs and the base plates of the Stewart plateform are replaced by flexible connections with high longitudinal stiffness and low bending stiffness (such flexible tips can be seen in Fig.3.5), in such a way that the stiffness matrix has an additional contribution, K_e, from the elastic joints. Thus,

$$K = kBB^T + K_e \tag{6.33}$$

and the closed loop equation becomes

$$[Ms^2 + K_e + kBB^T \frac{s}{s+g}]x = 0 \tag{6.34}$$

According to this equation, the transmission zeros, which are the asymptotic solutions of Equ.(6.34) as $g \to \infty$, are no longer at the origin ($s = 0$), but are solutions of the eigenvalue problem

$$[Ms^2 + K_e]x = 0 \tag{6.35}$$

This shift of the zeros may have a substantial influence on the practical performances of actual Stewart platforms.

(ii) The foregoing model assumes that the legs of the Stewart platform have no mass. In fact, the magnetic circuit of the voice coil actuator is fairly heavy and the local dynamics of the legs may interfere with that of the Stewart platform, resulting in a reduced attenuation of the isolation system.

6.8 Pointing control

At this stage, it is worth pointing out that, in addition to providing vibration isolation, a Stewart platform may also be used for pointing of, for example, a

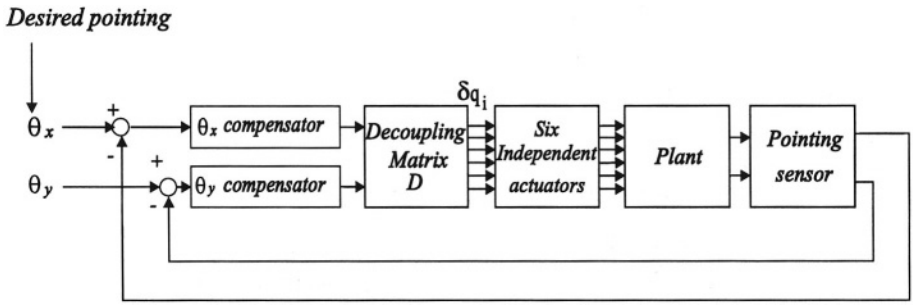

Figure 6.16: *Block diagram of the pointing control problem.*

telescope towards a target star (the reference pointing accuracy of the Hubble Space Telescope is $0.01 arcsec = 5\ 10^{-8} rad = 0.05 \mu rad$, but future missions are likely to require better accuracy by at least one order of magnitude).

If $\theta = (\theta_x, \theta_y)^T$ are the desired pointing angles, the decoupling matrix D relating θ to the corresponding leg extensions q in the nominal position is obtained from the appropriate columns of the Jacobian J.

$$\delta q = D \delta \theta \tag{6.36}$$

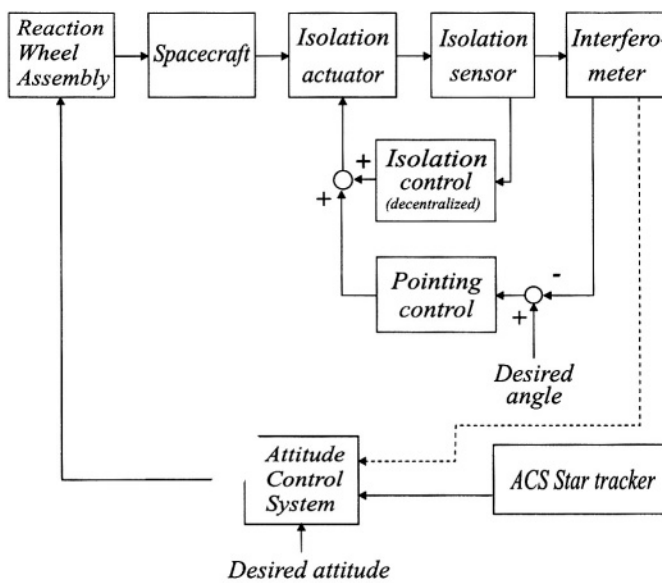

Figure 6.17: *Pointing/isolation control strategy for the 6 d.o.f. isolator.*

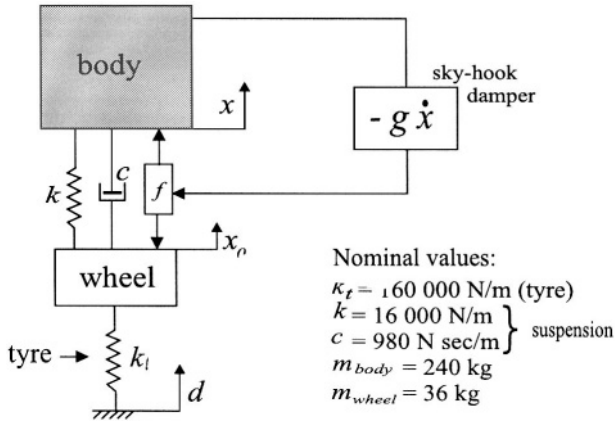

Figure 6.18: *Quarter-car model and sky-hook damper.*

Figure 6.16 shows a possible control strategy. Note that the six-leg Stewart platform has some built-in redundancy which can be exploited to account for actuator failure. Figure 6.17 shows the block diagram of the combined control strategy for pointing and isolation.

6.9 Vehicle suspension

Figure 6.18 shows a quarter-car model of a vehicle. Although this 2 d.o.f. model is too simple for performing a comprehensive analysis of the ride motion, it is sufficient to gain some insight in the behaviour of passive and active suspensions in terms of vibration isolation (represented by the body acceleration $\ddot{x}$), suspension travel $(x - x_0)$ and road holding (represented by the tyre deflexion $x_0 - d$). Typical numerical values used in the simulation reported later are also given in the figure (taken from Chalasani, 1984). The stiffness k_t corresponds to the tyre; the suspension consists of a passive part (spring k + damper c) and an active one, assumed to be a perfect force actuator acting as a sky-hook damper in this case (the active control force is applied on both sides of the active device, to the body and to the wheel of the vehicle).

Figure 6.19 shows the *FRF* from the roadway vertical velocity $\dot{d}$ to the car body acceleration $\ddot{x}$ for the passive suspension alone; several values of the damping coefficient c are considered. The first peak corresponds to the body resonance (also called sprung mass resonance) and the second one to the wheel resonance (unsprung mass resonance). The passive damping cannot control the body resonance without reducing the isolation at higher frequency.

Next, a sky-hook damper $(f = -g\dot{x})$ is added. Figure 6.20 shows the corresponding *FRF* from $\dot{d}$ to $\ddot{x}$ for various values of the control gain. Note that

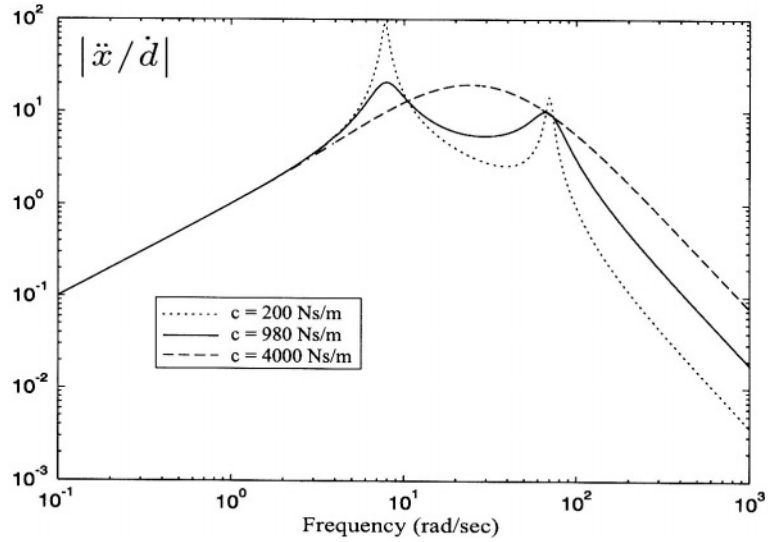

Figure 6.19: *FRF of the passive suspension ($\ddot{x}/\dot{d}$) for various values of the damping coefficient.*

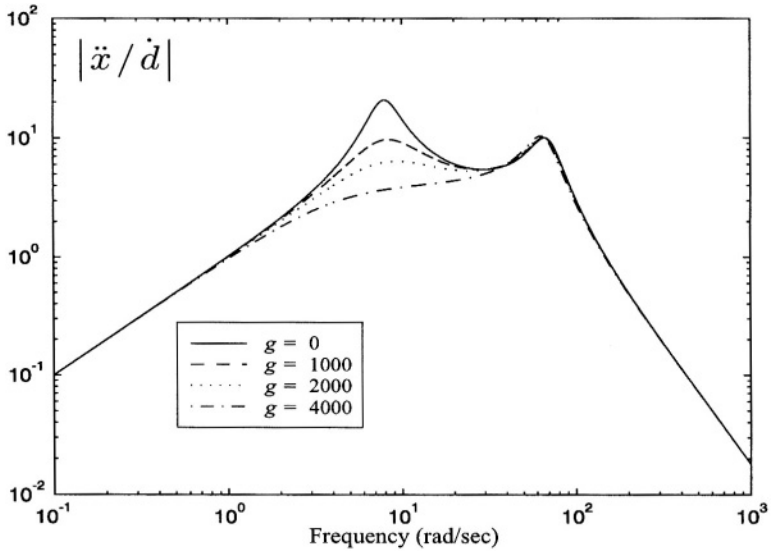

Figure 6.20: *FRF of the active suspension ($\ddot{x}/\dot{d}$) for various values of the gain g of the sky-hook damper (all the other parameters have the nominal values listed in Fig.6.18).*

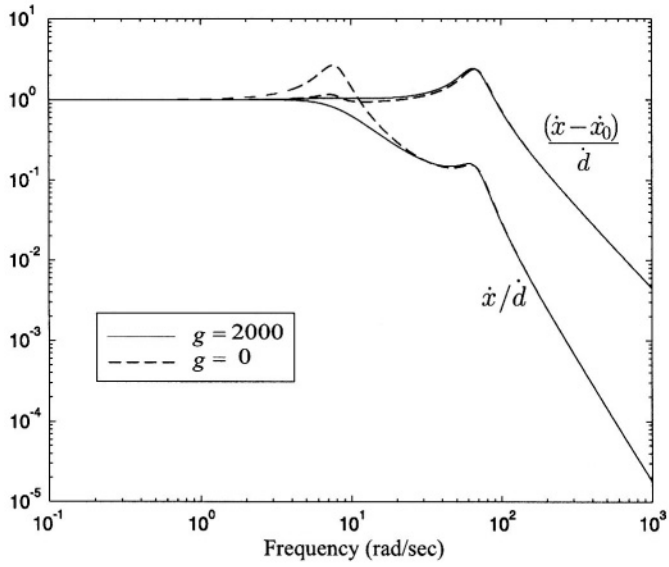

Figure 6.21: *Comparison of* $|\dot{x}/\dot{d}|$ *and* $|(\dot{x} - \dot{x}_0)/\dot{d}|$.

the body resonance can be damped without reducing the isolation at higher frequency but the peak in the *FRF* corresponding to the wheel resonance cannot be changed by the active control. Figure 6.21 compares the amplitude of the *FRF* $\dot{x}/\dot{d}$ and $(\dot{x} - \dot{x}_0)/\dot{d}$ for two values of the gain. This figure shows that the absolute velocity of the body $\dot{x}$ rolls-off much faster (i.e. has much lower frequency components) than the relative velocity $(\dot{x} - \dot{x}_0)$. This point will be further discussed when we examine the semi-active suspension devices which try to emulate the sky-hook damper by acting on the flow parameters of the damper acting on the *relative* velocity.

6.10 References

R. M. CHALASANI, Ride Performance Potential of Active Suspension Systems, Part1: Simplified Analysis Based on a Quarter-Car Model, ASME Symposium on Simulation and Control of Ground vehicles and Transportation systems, Anaheim, CA, Dec. 1984.

C. R. FULLER, S. J. ELLIOTT & P. A. NELSON, *Active Control of Vibration,* Academic Press, 1996.

Z. J. GENG & L. S. HAYNES, Six Degree-of-Freedom Active Vibration Control Using the Stewart Platforms, *IEEE Transactions on Control Systems Technology,* vol. 2, no. 1, 45–53, March 1994.

C. E. KAPLOW & J. R. VELMAN, Active Local Vibration Isolation Applied to a Flexible Space Telescope, *AIAA J. Guidance and Control,* vol. 3, no. 3, 227–233, May–June 1980.

D. KARNOPP, Design Principles for Vibration Control Systems Using Semi-Active Dampers, *Trans. ASME Journal of Dynamic Systems, Measurement and Control,* vol. 112, 448–455, Sep. 1990.

D. C. KARNOPP & A. K. TRIKHA, Comparative Study of Optimization Techniques for Shock and Vibration Isolation, *Trans. ASME, Journal of Engineering for Industry, series B,* vol. 91, no. 4, 1128–1132, 1969.

R. A. LASKIN & S. W. SIRLIN, Future Payload Isolation and Pointing System Technology, *AIAA J. Guidance and Control,* vol. 9, no. 4, 469–477, July–Aug. 1986.

J. E. Mc INROY, G. W. NEAT & J. F. O'BRIEN, A Robotic Approach to Fault-Tolerant, Precision Pointing, *IEEE Robotics & Automation Magazine,* pp. 24–31, Dec. 1999.

J. SPANOS, Z. RAHMAN & G. BLACKWOOD, A Soft 6-Axis Active Vibration Isolator, Proceedings of the American Control Conference, Seattle, WA, pp. 412–416, June 1995.

D. STEWART, A Platform with Six Degrees of Freedom, *Proc. Instn. Mech. Engrs,* vol. 180, no. 15, 371–386, 1965–66.

D. THAYER, J. VAGNERS, A. VON FLOTOW, C. HARDHAM & K. SCRIBNER, Six-Axis Vibration Isolation System Using Soft Actuators and Multiple Sensors, Proc. of Annual American Astronautical Society Rocky Mountain Guidance and Control Conference (AAS-98-064), pp. 497–506, 1998.

6.11 Problems

P.6.1 *Consider the passive isolator of Fig.6.1.b. Find the transmissibility* $X_c(s)/X_d(s)$ *of the isolation system.*

P.6.2 *Analyse the effect of the passive damping on the transmissibility of the sky-hook damper. Is it beneficial or detrimental?*

P.6.3 *Write the differential equations governing the system of Fig.6.7 in state variable form. Using the following values of the parameters:* $m = 1.1kg, M = 1.7kg, k = k_1 = 1.2\ 10^4 N/m, m_1 = 0.5kg, c_1 = 0Ns/m$. *Write the open-loop frequency response for the acceleration feedback* $(\ddot{x}_c)$ *and force feedback* (f) *configurations and draw the corresponding poles/zeros pattern. In both cases draw the root locus for an integral controller. Do the same for* $m_1 = 3.5kg$; *investigate the effect of structural damping.*

P.6.4 *Consider the modal expansion of the open-loop FRF of the system of Fig.6.10.d. Show that the residues are all positive and that this results in alternating poles and zeros.*

P.6.5 *Consider the cubic Stewart platform of Fig.6.14:*

(1) Using energetic considerations, show that the mass matrix M, the stiffness matrix K, and the control force influence matrix B are given by Equ.(6.22) to (6.24).

(2) Show that the natural frequencies are given by Equ.(6.25) and (6.26). [Hint: write the Jacobian J *relating the leg extension to the motion of the payload frame* $(\delta q = J\delta x)$. *The stiffness matrix is given by* $K = kJ^TJ = kBB^T$ *where* k *is the stiffness of one strut.*]

P.6.6 *Consider a Stewart platform of cubic architecture* $(L = 0.5m)$ *supporting an axisymetric payload such that* $m = 15kg, R_x = 0.4m, R_z = 0.56m, Z_c = 0.14m$.

(1) Select the spring stiffness k *in order to achieve a corner frequency of about* $10Hz$.

(2) Calculate the corresponding natural frequencies.

(3) Select the controller gain g *to achieve a reasonable damping ratio for the 6 modes.*

P.6.7 *Consider the active isolation problem described in the figure below, where* $\dot{x}_0$ *is assumed to be a white-noise process.*

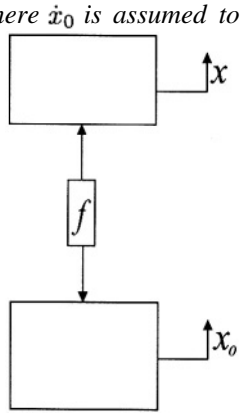

Show that the optimal control minimizing the objective function

$$J = c_1 E[\dot{x}^2] + c_2 E[(x - x_0)^2]$$

is

$$f = -b\dot{x} - k(x - x_0)$$

where *the coefficients* b *and* k *depend on the weighting coefficients* c_1 *and* c_2. *This is the "sky-hook" damper (Karnopp & Trikha, 1969). (The solution of this problem requires a prior reading of Chapters 7 and 9).*

P.6.8 *(1) Develop a state space model of the vehicle suspension of Fig.6.18 (use* $x, \dot{x}, x_0$ *and* $\dot{x}_0$ *as state variables).*

(2) Plot the amplitude of the FRF $|\ddot{x}/\dot{d}|$ *of the passive suspension for various*

values of the damping coefficient c. Compare with Fig.6.19.

(3) Consider the active suspension with a sky-hook damper control law. Plot the amplitude of the FRF $|\ddot{x}/\dot{d}|$ for the nominal parameters and various values of the gain g. Compare the frequency content of the absolute velocity of the body $\dot{x}$ with that of the relative velocity $(\dot{x} - \dot{x}_0)$.

P.6.9 *Consider the fully active suspension of Fig.6.18 $(k = c = 0)$. Using the LQR theory, design a state feedback which minimizes the performance index*

$$J = \int_0^\infty [\dot{x}^2 + \alpha(x - x_0)^2 + \beta\dot{x}_0^2 + \rho f^2]\, dt$$

The terms involved in the state penalty of this performance index represent respectively the vibration isolation (comfort), the suspension travel and the road holding (unsprung mass velocity). The fourth one is the control force. Try various values for the weighting coefficients α, β and ρ. Compare the full-state feedback to the sky-hook damper (Chalasani, 1984). (The solution of this problem requires a prior reading of Chapters 7 and 9).